Saharan dust and biomass burning aerosols during ex-hurricane Ophelia: validation of the new UK lidar and sun-photometer network

Martin Osborne[1,2], Mariana Adam[3], Joelle Buxmann[1], Jaqueline Sugier[1], Franco Marenco[1], and Jim Haywood[1,2]

[1]Met Office, FitzRoy Road,Exeter, Devon, EX1 3PB, United Kingdom
[2]University of Exeter, Laver Building, North Park Road, Exeter, Devon, EX4 4QE, United Kingdom
[3]National Institute for R&D in Optoelectronics INOE2000, Str. Atomistilor Nr. 409, Magurele, Ilfov, 077125, Romania

Correspondence: Martin Osborne (martin.osborne@metoffice.gov.uk)

Abstract. On 15-16 October 2017, ex-hurricane Ophelia passed to the West of the British Isles, bringing dust from the Sahara and smoke from Portuguese forest fires that was observable to the naked eye and reported in the national press. We report here detailed observations of this event using the UK operational lidar and sunphotometer network, established for the early detection of aviation hazards. The observations, taken continuously over a period of 30 hours, show a complex picture, dominated

5   by several aerosol layers at different times, and clearly correlated with the passage of different air-masses associated with the intense cyclonic system. A similar evolution was observed at several sites, with a time delay between them explained by their different location with respect to the storm. The event commenced with a shallow dust layer at 1-2 km in altitude, and culminated in a deep and complex structure that lasted 12 hours at each site, correlated with the storm's warm sector. For most of the time, the aerosol detected was mineral dust, as highlighted by depolarisation measurements, but an intense smoke layer was

10   observed towards the end of the event, lasting around 3 hours at each site. The aerosol optical depth (AOD) during the whole event ranged from 0.2 to 2.9, with the larger AOD correlated to the intense smoke plume. Such a large AOD is unprecedented in the United Kingdom according to AERONET records for the last 20 years. The Raman lidars permitted the measurement of the aerosol extinction coefficient at 355 nm, the particle depolarisation ratio (PDR) and the lidar ratio (LR), and made possible the separation of the dust (depolarising) aerosol from other aerosol types. A specific extinction has also been computed to

15   provide an estimate of the atmospheric concentration of both aerosols separately, which peaked at 500 +/- 100 μgm^{-3} for the dust and 600 +/- 100 μgm^{-3} for the smoke. Backtrajectories computed using the Numerical Atmospheric dispersion Modelling Environment (NAME) were used to identify the sources and strengthen the conclusions drawn from the observations. The UK network represents a significant expansion of the observing capability in Northern Europe, with instruments evenly distributed across Great Britain, from Camborne in Cornwall to Lerwick in the Shetland islands, and this study represents the first attempt

20   to demonstrate its capability and validate the methods in use. Its ultimate purpose will be the detection and quantification of volcanic plumes, but the present study clearly demonstrates the advanced capabilities of the network.

1 Introduction

Aerosol particles are ubiquitous in the Earth's atmosphere and play a fundamental role in the Earth's radiation budget as well as impacting human health and well being (e.g. Boucher et al., 2013; Mallone et al., 2011). In sufficient concentrations aerosols can also present significant hazards to aviation (Guffanti et al., 2010). For example, the 2010 eruption of the Icelandic volcano Eyjafjallajökull caused widespread disruption to air travell across Europe for several days, and had a significant financial impact (Gertisser, 2010). The large spacial and temporal variabilities in aerosol type and concentration makes their measurement and quantification a challenging task. Active laser remote sensing using lidars is well suited to this task as it provides atmospheric profiles that are highly resolved in both altitude and time. Lidar netwoks (e.g. EARLINET, LALINET and MPLNET (Pappalardo et al., 2004; Guerrero-Rascado et al., 2016; Lewis et al., 2016)) can also provide coverage over a wide geographical area, and can be used to track the evolution of aerosol plumes. By using lidars equipped with a Raman channel as well as depolarisation discrimination, aerosol identification can be attempted as well as the estimation of separate mass profiles for spherical and depolarising aerosols (e.g. Ansmann et al., 1992; Tesche et al., 2009; Groß et al., 2015a).

The Met Office acts as the London Volcanic Ash Advisory Centre (VAAC) and is responsible for issuing forecasts and information to the aviation community in the event of a volcanic eruption in the North Eastern Atlantic region. To consolidate its ash-aerosol remote sensing capability the Met Office has recently established a network of ten single wavelength, ground-based, N_2 Raman lidar installations across the UK. The installations also have co-located AERONET sun-photometers (Adam et al., 2017). During a volcanic event data from the new network will be used by VAAC forecasters and meteorologists to supplement model output as well as satellite observations and aircraft measurements from the Met Office Civil Contingencies Aircraft (MOCCA) (Millington et al., 2012; Francis et al., 2012; Marenco et al., 2011; Johnson et al., 2012). The ground based lidar / sun-photometer network will contribute to discriminating non-spherical ash particles from the predominantly spherical particles associated with industrial pollution. Aviation safety thresholds are set in terms of volcanic ash mass concentration, and in this paper we assess the ability of the lidar / sun-photometer network to deliver estimates of this quantity, as well as to distinguish between aerosol types. In the absence of volcanic eruptions, mineral dust is the most appropriate "proxy" for volcanic ash in terms of its size distribution and mineralogy, and hence its optical properties at solar (and terrestrial) wavelengths (Millington et al., 2012; Johnson et al., 2012; Turnbull et al., 2012). The DRIVE project (Developing Resilience to Icelandic Volcanic Eruptions) seeks to make this assessment by making opportunistic measurements of aerosol optical properties and mass concentrations, particularly during the mineral dust events which typically affect the UK around twice a year (Ryall et al., 2002). Where possible these measurements may be compared to in-situ aircraft observations made using MOCCA (Osborne et al., 2017). Measurements from the network are also relevant to the general study of aerosol optical properties. In particular, observations of aged mineral dust over northern Europe and the UK are lacking (Groß et al., 2015a), and are required to consolidate / improve aerosol classification schemes, for example that proposed for the EarthCARE mission (Groß et al., 2015b).

On 15th and 16th October 2017 un-usually large amounts of Saharan dust were transported to the UK in the warm conveyor-belt (Browning and Roberts, 1994) associated with the passage of ex-hurricane Ophelia across the Atlantic and then northward

along the west coast of Ireland. At the same time, wildfires in Portugal, fanned by the high winds associated with Ophelia, produced biomass burning aerosols which were also transported over much of the UK. This event attracted the attention of the UK national press for the yellow / sepia coloured skies and red sun it caused, and also because a number of flights were grounded due to pilots and passengers reporting a smell of smoke (BBC, 2017; Hecimovic, 2017).

5   In this paper we use observations made using the Met Office Raman lidars and sun-photometers, with additional data from AERONET and SKYNET sun-photometers, to characterise the aerosols present in the atmosphere over the UK during this event. We also present high quality measurements of aerosol lidar ratios and particle linear depolarization ratios. Back trajectories from the Met Office Numerical Atmospheric-dispersion Modelling Environment (NAME) are used to identify the source of the aerosols and estimate transport times. The case study presented here forms part of the ongoing validation and testing of

10   the new network and its capabilities.

The paper is organised as follows. In section 2 the lidar / sun-photometer network and retrieval methods are briefly described. In section 3 the synoptic meteorological situation and dust AOD forecast are presented. Section 4 presents and discusses the observations, while section 5 provides some conclusions.

2   Methods

15 ### 2.1   Raman lidar

The lidar network consists of nine fixed locations and one mobile facility (see locations shown in figure 1). The lidars, Raymetrics LR111-300s, are bespoke systems developed and manufactured to meet the Met Office and VAAC needs by Raymetrics located in Athens, Greece (website: https://www.raymetrics.com) . The instruments emit at 355nm and have polar and co-polar depolarisation detection channels at 355nm, and an N_2 Raman detection channel at 387nm. The systems use Quantel CFR 200

20   Q-switch-pulsed Nd:YAG lasers, with nominal pulse energies of 50mJ, and a repetition rate of 20Hz. Before leaving the lidar, the beam passes through a x7 beam expander making the emitted beam eye safe. The receiving telescope is a 30 cm diameter Cassegrain type, and full overlap between the emitted laser beam and the telescope field of view is achieved at around 250m. Alignment is ensured using the telecover test described in Freudenthaler et al. (2018). Polarisation discrimination is made via a polarisation beam splitter cube, with additional clean sheet filers placed after the cube to ensure cross talk between the

25   channels is negligible. During callibration the wavelength and polarisation separation optics can be rotated to pre-set positions, and the polarization channels of each lidar are calibrated using the + / - 45 degree procedure from Freudenthaler et al. (2009) and as detailed in Buxmann et al. (2017). The detectors are Hamamstsu R9880-U110 photo multiplier tubes (PMTs) and data acquisition is made using a Licel TR-20 transient recorder. Data is acquired in both analogue and photon-counting modes. Each lidar can be operated remotely from the Met Office Exeter headquarters (Adam et al., 2017). Data from the lidars are

30   transmitted to the Met Office headquarters and can be accessed and visualized in near real time in the VAAC. In the future data from the lidars will be made available on the Centre for Environmental Data Analysis (CEDA) data repository with a 48 hours delay; however, at the time of writing this facility is yet to be implemented.

2.2 Lidar retrievals

Aerosol optical properties are calculated from lidar analogue and photon counting signals using code developed at the Met Office, and which has been tested against the EARLINET Single Calculus Chain (SCC) (D'Amico et al., 2016; Mattis et al., 2016) and found to be in agreement. In common with SCC, errors are estimated using a Monte-Carlo method.

5   During hours of darkness, extinction and backscatter profiles are derived independently using the Raman and elastic channels (Ansmann et al., 1990, 1992), and hence both the aerosol lidar ratio (LR) and the particle linear depolarisation ratio (PDR) can be measured. During day-light hours the Raman channel cannot be relied upon, as it is affected by shot noise. Therefore, during day-light hours the aerosol properties are computed using the elastic channels only, meaning that a constrain on the LR has to be used a priori. A constraint can be placed on the LR, for example by assuming that the LR measured in the night also

10 applies in daytime, or by ensuring consistency of the lidar-derived AOD with the sun-photometer measurements.

     In this study we have also made use of day-time Raman measurements during a period of high aerosol optical depth. This has been done in the follwing way. The Raman channel was used to derive the first 2km of the extinction profile in the normal way as in Ansmann et al. (1990), where no reference range is needed. The backscatter profile could not be retrieved in the normal way, as in Ansmann et al. (1992) where the ratio of the Raman and elastic signals is used, as no molecular only reference range

15 could be found in the Raman signal (the far end being masked by the background signal as described above). In order to find a reference range within the first 2km it was therefore necessary to know the value of the aerosol backscatter coefficient at some height. Kovalev (1993) provides a method of finding the aerosol extinction profile from elastic only lidar data (without the use of a reference range) by constraining the solution using the total optical depth. This method can be applied to a small vertical section of the lidar signal if the optical depth in that section is known and, in the case of a Raman lidar, this can readily be

20 computed by integrating the Raman derived aerosol extinction profile within the desired section. The Kovalev method requires the assumption of LR. Any realistic value may be chosen, each value results in a different vertical distribution for the aerosol extinction profile. As we already have a "true" aerosol extinction profile from the Raman channel, it is possible to fix the most appropriate aerosol lidar ratio by finding the value which minimises the differences between the Raman derived aerosol extinction profile and that resulting from the Kovalev method within the small vertical section under consideration. A well

25 mixed 400m section, within which the lidar ratio is expected to be constant, was chosen to perform this process. Having found the most appropriate lidar ratio, a single height, within the 400m section, was chosen to convert the Raman derived aerosol extinction value to backscatter by dividing by the lidar ratio. This point is then used as the reference range and first 2km of the backscatter profile was found as in Ansmann et al. (1992). Using this method it has been possible to make measurements of PDR and LR in the lower 2km of the atmosphere during day-light hours.

30   In each retrieval distinct layers were identified, with reference to the backscatter and particle linear depolarisation profiles. Values for specific extinction [K_{ext}] calculated from sun-photometer data (see next section) were used, together with the lidar extinction and PDR data, to obtain separate mass concentration profiles for fine and coarse mode aerosols (Tesche et al., 2009). When performing this separation we have assumed constant depolarization ratios for coarse mode and fine mode aerosols of 26% (dust like), and 5% (pollution / biomass burning / marine like) respectively (Ansmann et al., 2012; Groß et al., 2015a).

The mass retrievals are sensitive to the choice of depolarisation ratios, and we have chosen these based on values measured during this study in layers we are reasonably sure contained only one type of aerosol.

2.3 Sun-photometer network / Specific extinction

Co-located with the lidars are Cimel CE318 multiband sun-photometers. The instruments make direct sun observations of
5 aerosol optical depth at several wavelengths. Under cloud free conditions the instruments also make off sun almucanter scans from which aerosol size distributions are inverted (Holben et al., 1998). In common with the lidars, data from the sun-photometers are transmitted to the Met Office headquarters and can be accessed and visualized in near real time. However, in the case of the sun-photometers, data are also processed by AERONET and made available on their website.

In this study we have also made use of sun-photometer data from other AERONET federated Cimel sun-photometers -
10 specifically those at Rame Head, Bayfordbury, Edinburgh and FZJ JOYCE in Germany. We also make use of data from a Prede-POM sun-photometer. This instrument is part of the SKYNET sun-photometer network (Tackamura et al., 2004), and uses the SKYRAD package to provide aerosol optical depths and aerosol size distributions. The Prede-POM sun-photometer is currently co-located with the Rame Head AERONET sun-photometer on the roof of the Plymouth Marine Laboratory building in Plymouth (Estellés et al., 2012).

15 As well as volume concentrations for fine and coarse mode aerosols, the AERONET processing algorithm reports individual optical depths for fine and coarse mode aerosols. Following the techniques described in Ansmann et al. (2011) this information was combined to calculate values for fine and coarse mode specific extinction K_{ext}.

In contrast to AERONET, SKYNET does not provide separate values for fine and coarse mode AODs. Therefore, to obtain a value for coarse mode K_{ext} from the SKYNET data, separate fine and coarse mode optical depths were calculated in the
20 following way. Firstly for each SKYNET size distribution log-normal modes were fitted using the Gaussian mixture model described in Taylor et al. (2014). A good fit was achieved with three modes. The log-normal fit corresponding to the fine mode was then used in scattering calculations to calculate a fine mode optical depth, which was then subtracted from the total optical depth to arrive at a value for the coarse modes. In order to be consistent with the calculations used by AERONET, we used T-Matrix calculations for randomly orientated spheroids, averaged over aspect ratios ranging from 0.4 to 2.49. Finally, the
25 resulting values for fine and coarse mode optical depths, together with the volume concentrations for each mode, were used as in Ansmann et al. (2011) to calculate K_{ext}.

As a sanity check, the same calculations were made for the co-located AERONET fine mode size distributions from Rame Head. Fine mode AODs calculated using a refractive index of 1.45-0.01i were found to match the measured AERONET fine mode AOD almost exactly. This refractive index is representative of values found in the literature for industrial aerosol
30 dominated by sulphate from pollution mixed with black carbon (Raut and Chazette, 2007; Levin et al., 2010; Poudel et al., 2017), and this value was therefore used in the calculations for the SKYNET POM fine mode optical depths.

3 Meteorological situation and dust AOD forecast

3.1 Ex-hurricane Ophelia

Figure 2 shows a Met Office synoptic forecast chart for midnight on the 16th October 2017. Ex-hurricane Ophelia can been seen as a low pressure system to the south west of Ireland. Originating in a decaying cold front in the Eastern Atlantic, Ophelia

5   became a hurricane in the 11th October, before strengthening to a major hurricane on 14th and moving North East towards Ireland. With winds exceeding $50ms^{-1}$, Ophelia is the farthest east storm reaching such intensity on record (US National Hurricane Center, 2017). The chart also shows a warm front associated with Ophelia passing over Ireland and the UK, followed by a warm sector, a cold front and a following cold sector. Within the warm sector, the w arm conveyor feeding warm air into the cyclonic system also drew air masses up from the West African coast to the UK, and on the 16th in particular, drew air

10   masses from regions with active forest fires in Portugal. Late on the 15th October, the storm weakened as it passed over the colder waters towards Ireland. Ophelia made land fall in Ireland on 16th October as an extremely violent storm, with winds reaching $35ms^{-1}$(Hurricane force) in County Cork. The storm then tracked North East over the UK before dissipating over Scandinavia.

Figure 3 shows MODIS Aqua images from the North Atlantic region for the 14th, 15th, 16th and 17th October 2017. Ophelia

15   is highlighted in red in the first three pannels. On the 14th a plume of Saharan dust can be seen off the coast of Mauritania and Western Sahara, and by the 15th the warm sector and cold front are passing over this plume, likely entraining a proportion of it and transporting it northwards. Aerosols can be seen in the warm sector ahead of Ophelia. By the 16th the cold front and warm conveyor are passing over the UK and Portugal. By the 17th Ophelia has dissipated and a distinctive greyish plume can be seen in MODIS imagery (panel 4, figure 3) over Northern France, Belgium, and Northern Germany. We interpret this as the

20   residual aerosol cloud from this event, and Aeronet data measured through this plume over Germany will be used to support our results and conclusions.

3.2 Dust forecasts

As part of the DRIVE project, dust AOD forecasts from the Met Office Unified Model (MetUM) and the Copernicus Atmosphere Monitoring Service (CAMS) model are monitored daily. Operational dust forecasts have been developed from the

25   original dust mobilisation, transport and deposition scheme developed by Woodward (2001) and have been shown to compare favourably in the immediate vicinity of the Sahara desert (Greed et al., 2008). The scheme for transport has since been adapted to a two bin scheme in order to improve computational efficiency (although in this study the dust uplift scheme remains the same, with dust generated in 6 bins). Figure 1 shows output from the Met Office operational dust forecast from midnight UTC on 13th October 2017 for a validity time of 9am on 16th October 2017 (T+81hours). The forecast shows a

30   dust plume covering most of the UK with a maximum dust AOD_{550} of 0.28. The CAMS forecast (available from ECMWF (https://atmosphere.copernicus.eu/) predicted a similar distribution of dust but with a higher maximum dust AOD_{550} between 0.4 and 0.5.

4 Results and discussion

4.1 Lidar observations

Lidar measurements began at 11:00 on 15th October 2017 and they were continued until 17:00 the following day. Figure 5 shows the volume linear depolarisation ratio (VDR) for four lidar stations (locations are shown in figure 1). Other lidars in the network did not record useful data due to rain or very low cloud, and rain also prevented measurements being made at Camborne for much of the 16th. In figure 5 the four panels are arranged with the westerly most station (Camborne) at the top and then moving progressively east in the three panels below showing the passage of the warm front, warm sector and cold front as they tracked from west to east across the UK. A layer of depolarising aerosol arrived over Camborne, Rhyl and Loftus on the morning of the 15th October between 1km and 2 km. This plume was ahead of the warm front and was followed 12 hours later by a much thicker plume extending from 1km to 6km, well identified at the four locations, although with different timing. The beginning of this plume marks the arrival of the warm front, and the wedge shaped profile is typical of an advancing warm front being undercut by colder air. The thicker plume was in the warm sector associated with Ophelia's warm conveyor, and persisted for around 12 hours. Towards the later three hours of this plume, and still in the warm sector, an optically very thick layer arrived, initially at around 1km, and later ascending to 2km. This optically thick layer was less than 1km in vertical extent and marked the end of the warm sector and the arrival of the cold front. Again the profile has a distinctive wedge shape, this time caused by advancing colder air undercutting the warm air associated with the warm conveyor. The cold sector is largley free of strongly depolarising aerosols with the exception of a thin layer at the top of the boundary layer, initially at 1km and rising to 2km.

Similar features can be seen in each panel, but shifted in time, showing the progress of the warm sector and associated dust plume west to east. At all four sites, there was a strong, only slightly depolarising, boundary layer (showing a strong total elastic signal - not shown here). The boundary layer was mostly confined to the lower 1km, rising sightly to 2km after the cold front had passed.

4.2 Sun-photometer AODs

The available sun-photometer AOD measurements are shown in the upper two pannels of figure 6. Please note the break in the y-axis. With the exception of the four data points plotted as triangles on the 16th (see below) the AERONET data is cloud screened level 1.5 data processed by version 3 of the AERONET algorithm. Only four of the ten Met Office sun-photometers (those at Portglenone, Loftus, Watnall and East Malling) were able to make measurements that survived the AERONET cloud screening. The additional AERONET sun photometers at Bayfordbury, Rame Head and Edinburgh were also able to collect data, as was the SKYNET Prede POM sun-photometer. As described above, this latter instrument was co-located with the Rame Head AERONET sun-photometer.

The AOD$_{500}$ measured on the 15th October by the more southerly instruments - Rame head, PML, Bayfordbury, and East Malling - show similar values and variation. Inspection of figure 5 suggests that these measurements were made when the thinner aerosol layer ahead of the warm front was overhead, and before the arrival of the thicker plume. Edinburgh, Portglenone

and Loftus, where the AOD_{500} was often below 0.1, are the more northerly instruments, and it is likley that the first aerosol plume did not reach these locations until after 3pm on the 15th (see lidar data for Loftus in figure 5).

On the morning of the 16th the PML sun-photometer recorded an AOD_{500} of 1.1, and later, the Watnall and Loftus sun-photometers recorded AOD_{675}s of 2.8 (10:36am) and 2.3 (12:35pm) respectively. To put this into context, the entire UK catalogue of level 1.5 AERONET AODs at 500nm or 675nm running from 1997 to 2017 contains no values greater than around 1.75. The high AOD measured on the 16th October are therefore exceptional.

On the 16th the AERONET level 1.5 cloud screening had removed all data points before 14:00UTC at Watnall and Loftus. However, the non-cloud screened data from these sites contain two measurements of AOD_{500} each - 2.9 and 2.5 at Watnall, and 1.48 and 2.27 at Loftus. These data are plotted in figure 6 as triangles. The Angstrom exponents at these times were 1.6, 0.9, 1.7 and 0.8 respectively. Angstrom exponents of this size indicate that the particles present were small. This would not be the case if the optical depth had been due to cirrus cloud, which is composed of very large ice particles that produce almost no wavelength variation in AODs at visible wavelengths.

Further evidence that these very high AOD measurements are not due to cloud is provided by AERONET measurements from more easterly sites on the 17th October. The MODIS imagery in figure 3 shows that the aerosol plume and warm sector moved over mainland Europe on the 17th October, and impacted AERONET sites in Northern Europe. AOD_{500} values of upto 2.4 are found in the level 1.5 AERONET data for sites in Lille, Brussels and Julich in Germany, which are comparable to the level 1.0 AOD values at Watnall and Loftus. Corresponding Angstrom exponents of upto 1.2 are also similar to those in the level 1.0 data at Watnall and Loftus. It is possible that the cloud screening of the UK AERONET data has been susceptible to the inhomogeneity of an unusually optically thick aerosol layer (AOD_{500} upto 2.9), and has discarded un-contaminated data, or the presence of patchy cloud has caused data rejection. As an example, figure 7 shows the wavelength dependent Level 2.0 AOD derived from the AERONET station at Jeulich in Germany on the 17th October. The very high AODs exceeding 2 are more clearly evident as the impacts of cloud contamination are less than over the UK on the 16th October. Thus we are confident that the Level 1.0 AODs over the UK are accurate, and that the high AOD_{500} measurements at Watnall and Loftus are in-fact not contaminated by cloud, and are a true measurement of the aerosol optical depth. As we will shown in section 4.4, a lidar derived optical depth at Watnall, coincident with the sun-photometer AOD_{500} measurement of 2.9, is of a similar magnitude.

Inspection of figure 5 shows that the very high AODs measured at Watnall and Loftus were associated with the end of the warm sector plume. The AOD at all sites dropped to around 0.2, after the warm sector plume and cold front have passed.

4.3 Sun-photometer size distributions and Specific extinction

The lower panel of figure 6 shows the available sun-photometer derived volume size distributions for the 15th and 16th October 2017. The majority of the size distributions were measured on the 15th and correspond to the initial thinner plume of mineral dust influenced aerosol in the cold sector ahead of the warm front. While the co-located Rame Head and PML SKYNET instruments show good agreement for AOD, the size distributions are significantly different. Most notably, above 10μm the AERONET size distributions quickly approach zero, while the SKYNET size distributions do not. The SKYNET size distribu-

tion is also tri-modal while the AERONET size distributions are bi-modal. These differences have been noted before (e.g. Che et al., 2008; Estellés et al., 2012), and as shown below, these differences have an impact on specific extinction values.

One size distribution was measured in the warm sector - at Bayfordbury at 10:12 on the 16th (dark blue curve - diamond markers in figure 6). The effective radius of the coarse mode of this size distribution is slightly smaller than those of the coarse

5   modes measured in the cold sector ahead of the warm front, and, as is shown below, the specific extinction is correspondingly larger. This size distribution also shows a more prominent fine mode volume. One size distribution was measured after the cold front had passed - at Watnall at 14:53 on the 16th (light blue curve / square markers in figure 6). The shape of the coarse mode is markedly different to those from either the earlier cold sector or the warm sector, with a much broader width. Again, the specific extinction for this mode is different to those in either of the preceding sectors.

10   The values for coarse mode specific extinction obtained are listed in table 1. In the initial plume on the 15th, the mean value of K_{ext} calculated using the AERONET data from all locations was $0.56\pm0.02\mathrm{m^2g^{-1}}$, and that found using the SKYNET data was $0.41\pm0.03\mathrm{m^2g^{-1}}$. The K_{ext} value calculated using the one size distribution from the warm sector is $0.65\mathrm{m^2g^{-1}}$, indicating that the coarse mode aerosols in the warm sector contains smaller, more effective scatterers than those in the preceding cold sector. The value of K_{ext} in the later cold sector was $0.48\mathrm{m^2g^{-1}}$.

15   The values reported here are within the range reported in the literature for coarse dust aerosols, but also for volcanic ash from the Eyja eruption indicating indicating the similarity in size distribution (e.g. Clarke et al., 2004; Osborne et al., 2008; Johnson et al., 2012; Ansmann et al., 2012; Nemuc et al., 2013).

4.4   Aerosol classification and mass concentrations

The lidar retrievals are summarised in table 2 - optical properties and mass concentrations were derived from lidar measure-
20   ments averaged between the times indicated. The Table is divided into three subsections, corresponding to retrievals made in the initial cold sector, the following warm sector, and the final cold sector. The AOD of each layer was calculated by integrating the corresponding section of the lidar extinction profile. The PDR and LR values (measured using a combination of elastic and Raman signals) reported are the backscatter weighted mean values within each layer. Where n/a is listed the retrievals were made using the elastic signal only, without an AOD constraint, and hence no information on the lidar ratio was available. The
25   LR, together with the PDR have been used to attempt a classification of the aerosols based on a classification scheme such as that provided in Groß et al. (2015b) figure 2.

The aerosols in the thin depolarising layer in the initial cold sector had a mean PDR of $26\pm1.3\%$, and a mean LR of $43.3\pm5\mathrm{sr}$. These values suggest a layer of pure transported mineral dust. The peak concentration in this layer was estimated over Watnall at around 7pm and was $500\pm100\mu\mathrm{gm^{-3}}$. Below this the boundary layer had mean PDR of $5.75\pm2.8\%$, and a mean lidar ratio
30   of $35.3\pm5.4\mathrm{sr}$ suggesting either biomass burning aerosol or continental pollution or a combination of both (e.g. Groß et al., 2015a).

The deep and strongly depolarizing layer immediately after the warm front had a mean PDR of $26\pm2\%$, and a mean LR of $39\pm1\mathrm{sr}$ (see panel 1 in figure 8 - this example from the Watnall lidar 2:00am to 3:15am on the 16th). These values again indicate a layer of pure transported mineral dust. The peak mass concentration was $200\pm50\mu\mathrm{gm^{-3}}$. Around three to four hours

later the aerosol plume in the warm sector presents a more complicated structure. Row 2 of figure 8 shows the lidar profiles from Watnall 5:43am to 5:56am on the 16th. The lidar data reveals three distinct layers. The low mean PDR of 9±3% and LR of 28±5sr in the layers below 5km are consistent with a mixture of marine and dust aerosols. The layers above 5km have a similar PDR, but a higher LR 54±13sr and we identify this layer as a mixture of dust and biomass burning aerosols. The total

5 AOD, calculated by integrating the extinction profile from ground to 7km, was 0.88.

Row 1 of figure 9 shows the lidar profiles near the end of the warm sector plume and coincident with the very high AOD_{500} of 2.9 measured by the Watnall sun-photometer. The retrievals here have been made using both the Raman and elastic channels in the manner described in section 2.2. The lidar ratio, estimated by using the combination of the Raman extinction profile and the Kovalev method between 500m and 900m was 22 sr. The high backscatter signal, combined with the lower sky background

10 levels caused by the high optical depth have made this day-time use of the Raman data possible. An optically thick layer between 1km and 2km had a PDR of 5±1% and a LR of 58±5sr. These values are consistent with biomass burning aerosols. Given the exceptional AODs, and the expectation of dust and smoke, we identify this layer as a mixture of biomass burning aerosols and transported desert dust. An elastic only retrieval at the same time (figure 10) revealed further aerosol layers upto 5km, and a total AOD_{355} of 3.18. This of a similar magnitude to the AOD_{500} of 2.9 measured at the same time.

15 After the cold front had passed, the optically and geometrically thin depolarizing layer at around 1.5km had a mean PDR of 20±5%, consistent with a dusty mixture, and the depolarising layer above this at around 2.5km had a mean PDR of 28±5%, consistent with transported desert dust. The PDR value in this higher layer reached 33% at Watnall (Row 2, figure 9), the highest measured in this study.

4.5 Back trajectories and aerosol sources

20 Having classified the observed aerosol layers using the lidar and sun-photometer data, back trajectory analysis was used to validate the identifications. Figure 11 shows NAME back-trajectories for air masses arriving over Watnall at 3am on the 16th October (left hand panel) and 12pm on the 16th October (right hand panel). In the upper panels the trajectories are overlaid on an RGB tile from MODIS AQUA for the 16th October, with active forest fires (MODIS terra brightness temperature anomalies) shown as red spots. The symbols on each line in the upper panels show the positions at midnight on each day. The lower panel

25 shows the altitude of each trajectory. Trajectories that arrive at Watnall above 1km are plotted in magenta, and those bellow 1km are plotted in cyan. Note that the cloud above the UK has a brownish colour, supporting the presence of absorbing aerosols above the cloud that reduces the local planetary albedo and acts to warm the climate (Keil and Haywood, 2003).

The back trajectories arriving over Watnall at 3am suggest that the source region for the dust plume in the warm sector was western Algeria. This is supported by the SEVIRI dust RGB product (not shown) which shows the dust being lifted in this

30 region. Having been lifted on the 12th October, the dust was transported to the African coast by the morning of the 14th (see MODIS images in figure 3), before being caught in the warm conveyor associated with Ophelia on the 15th, and being quickly transported from 35° north to the UK in under 24 hours. The trajectories indicate that the air masses did not pass over the Iberian peninsular where a high density of active forest fires were located. In contrast, the lower layers were transported over continental Europe, but again did not bring air masses from areas with lots of forest fires.

The right hand panel in figure 11, the air masses arriving over Watnall at 12pm on the 16th pass over Portugal and an area with many active forest fires. A number of the trajectories arrive over this area on the morning of the 14th, and remain over Portugal for two days before being caught in Ophelia's warm conveyor and being transported to the UK in under 12 hours. These air masses coincide with the optically very thick layer identified in the previous section as biomass burning aerosols.

5 Summary and Conclusions

This study has presented measurements from a recently operational Raman lidar and sun-photometer network made during an exceptional event on the 15th and 16th October 2017. These measurements, supplemented by measurements from AERONET and SKYNET sun-photometers, have been used to classify the aerosols present and estimate their concentrations. MODIS imagery and NAME back trajectories have then been used to identify the likely aerosol sources.

Three sectors were identified. On the 15th October an initial cold sector ahead of ex-hurricane Ophelia contained a layer of Saharan dust. This was followed late on the 15th / early 16th by a warm front and warm sector which contained an initial thick plume of Saharan dust, followed by mixtures of dust and marine aerosols between 1km and 4km, and dust and biomass burning aerosols at around 6km. Following this, towards the end of the warm sector an optically very thick layer of biomass burning aerosols was observed, with an AOD of 1.3 for this layer alone. The total AOD measured by both lidar and sun-photometers at this time was in excess of 2.5. In comparison with the UK back-catalogue of sun-photometer AODs these are exceptionally high values. After the warm sector had passed, a trailing layer of highly depolarising Saharan dust was observed.

An analysis of back trajectories and MODIS imagery indicates that the source of the dust was western Algeria on the 12th October. This dust was then entrained by Ophelia's warm conveyor on the 15th October and transported from the African coast to the UK in under 24 hours. A similar analysis indicates that an optically thick layer (AOD 2.9) may have originated in an area of active forest fires in Portugal, and that the aerosols were transported from the Iberian peninsula to the UK in under 12 hours. It is interesting to note that under the majority of meteorological conditions, subsequent to emission, aerosol plumes become less concentrated as time progresses owing to divergent flow. However, the convergent flow in warm conveyors associated with cyclonic systems can act to concentrate aerosol plumes. "River of Smoke" events are quite commonly observed during the African biomass burning season and are associated with tropical-extra-tropical transport associated with the passage of cyclonic systems (Swap et al., 2000). However, this is the first time that a "River of Smoke" event has been documented over Europe.

Over all measurements, the mean PDR in layers identified as dust was 26.2±3%, and the mean LR was 43.3±5.2sr. These values are in agreement with those reported in the literature for transported Saharan dust. In the optically thick biomass burning layer, the mean PDR was 5±1% and the mean LR was 58±5sr, again these values are consistent with those reported in the literature for biomass burning aerosol.

This study represents the first published assessment of the new lidar / sun-photometer network, and is part of an ongoing program of testing and validation. The results presented here show that it is capable of aerosol classification, and the retrieval of

estimates of aerosol mass concentrations. To our knowledge this is the first operational Raman lidar / sun-photometer network owned and operated by a national meteorological service.

Competing interests. The authors declare that they have no conflict of interest

Acknowledgements. We thank the following PIs for their effort in establishing and maintaining the AERONET sites used in this study: Birger
5   Bohn (Institue für Energie und Klimaforschung - FZJ Joyce), Iain H. Woodhouse (University of Edinburgh - Edinburgh), Joseph Ulanowski (University of Hertfordshire - Bayfordbury) and Tim Smyth (Plymouth Marine Laboratory - Rame Head). We also thank Tim Smyth and Plymouth Marine Laboratory and the NERC National Capability funded Western Channel Observatory for the SKYNET POM data. We would like to thank all the Met Office teams involved in the VA Lidar-sunphotometer project. We are grateful to the Civil Aviation Authority and Department for Transport for funding the lidar / sun-photometer project. Funding for PhD work for Osborne was provided by the U.K.
10   Natural Environment Research Council through the University of Exeter - Grant NE/M009416/1

References

Adam, M., Buxmann, J., Freeman, N., Horseman, A., Slamon, C., Sugier, J., and Bennett, R.: The UK Lidar-Sunphotometer Operational Volcanic Ash Monitoring Network, in: Proceedings of the 28th International Laser Radar Conference, 2017.

Ansmann, A., Riebesell, M., and Weitkamp, C.: Measurement of atmospheric aerosol extinction profiles with a Raman lidar, Opt. Lett., 15, 746–748, https://doi.org/10.1364/OL.15.000746, http://ol.osa.org/abstract.cfm?URI=ol-15-13-746, 1990.

Ansmann, A., Wandinger, U., Riebesell, M., Weitkamp, C., and Michaelis, W.: Independent measurement of extinction and backscatter profiles in cirrus clouds by using a combined Raman elastic-backscatter lidar, Appl. Opt., 31, 7113–7131, https://doi.org/10.1364/AO.31.007113, http://ao.osa.org/abstract.cfm?URI=ao-31-33-7113, 1992.

Ansmann, A., Tesche, M., Seifert, P., Groß, S., Freudenthaler, V., Apituley, A., Wilson, K. M., Serikov, I., Linné, H., Heinold, B., Hiebsch, A., Schnell, F., Schmidt, J., Mattis, I., Wandinger, U., and Wiegner, M.: Ash and fine-mode particle mass profiles from EARLINET-AERONET observations over central Europe after the eruptions of the Eyjafjallajökull volcano in 2010, Journal of Geophysical Research: Atmospheres, 116, n/a–n/a, https://doi.org/10.1029/2010JD015567, http://dx.doi.org/10.1029/2010JD015567, d00U02, 2011.

Ansmann, A., Seifert, P., Tesche, M., and Wandinger, U.: Profiling of fine and coarse particle mass: case studies of Saharan dust and Eyjafjallajökull /Grimsvötn volcanic plumes, Atmospheric Chemistry and Physics, 12, 9399–9415, https://doi.org/10.5194/acp-12-9399-2012, https://www.atmos-chem-phys.net/12/9399/2012/, 2012.

BBC: Smoke smell forces flights to land at UK airports, BBC News, 16th October, http://www.bbc.co.uk/news/uk-england-41639386, 2017.

Boucher, O., Randall, D., Artaxo, P., Bretherton, C., Feingold, G., Forster, P., Kerminen, V.-M., Kondo, Y., Liao, H., Lohmann, U., Rasch, P., Satheesh, S., Sherwood, S., Stevens, B., and Zhang, X.: Clouds and Aerosols. In: Climate Change 2013: The Physical Science Basis. Contribution of Working Group I to the Fifth Assessment Report of the Intergovernmental Panel on Climate Change [Stocker, T.F., D. Qin, G.-K. Plattner, M. Tignor, S.K. Allen, J. Boschung, A. Nauels, Y. Xia, V. Bex and P.M. Midgley (eds.)]. Cambridge University Press, Cambridge, United Kingdom and New York, NY, USA., 2013.

Browning, K. and Roberts, N.: Structure of a frontal cyclone, Quarterly Journal of the Royal Meteorological Society, 120, 1535–1557, https://doi.org/10.1002/qj.49712052006, https://rmets.onlinelibrary.wiley.com/doi/abs/10.1002/qj.49712052006, 1994.

Buxmann, J., Adam, M., Georgoussis, G., Louridas, A., Horseman, A., and Sugier, J.: Calibration of the depolarisation channel of UV Raman lidar, in: Proceedings of the 28th International Laser Radar Conference, 2017.

Che, H., Shi, G., Uchiyama, A., Yamazaki, A., Chen, H., Goloub, P., and Zhang, X.: Intercomparison between aerosol optical properties by a PREDE skyradiometer and CIMEL sunphotometer over Beijing, China, Atmospheric Chemistry and Physics, 8, 3199–3214, https://doi.org/10.5194/acp-8-3199-2008, https://www.atmos-chem-phys.net/8/3199/2008/, 2008.

Clarke, A. D., Shinozuka, Y., Kapustin, V. N., Howell, S., Huebert, B., Doherty, S., Anderson, T., Covert, D., Anderson, J., Hua, X., Moore, K. G., McNaughton, C., Carmichael, G., and Weber, R.: Size distributions and mixtures of dust and black carbon aerosol in Asian outflow: Physiochemistry and optical properties, Journal of Geophysical Research: Atmospheres, 109, https://doi.org/10.1029/2003JD004378, http://dx.doi.org/10.1029/2003JD004378, d15S09, 2004.

D'Amico, G., Amodeo, A., Mattis, I., Freudenthaler, V., and Pappalardo, G.: EARLINET Single Calculus Chain – technical – Part 1: Pre-processing of raw lidar data, Atmospheric Measurement Techniques, 9, 491–507, https://doi.org/10.5194/amt-9-491-2016, https://www.atmos-meas-tech.net/9/491/2016/, 2016.

Estellés, V., Smyth, T. J., and Campanelli, M.: Columnar aerosol properties in a Northeastern Atlantic site (Plymouth, United Kingdom) by means of ground based skyradiometer data during years 20002008, Atmospheric Environment, 61, 180 – 188,

https://doi.org/https://doi.org/10.1016/j.atmosenv.2012.07.024, http://www.sciencedirect.com/science/article/pii/S1352231012006966, 2012.

Francis, P. N., Cooke, M. C., and Saunders, R. W.: Retrieval of physical properties of volcanic ash using Meteosat: A case study from the 2010 Eyjafjallajökull eruption, Journal of Geophysical Research: Atmospheres, 117, https://doi.org/10.1029/2011JD016788, https://agupubs.onlinelibrary.wiley.com/doi/abs/10.1029/2011JD016788, 2012.

Freudenthaler, V., Esselborne, M., Wiegner, M., Heese, B., Tesche, M., Ansmann, A., Muller, D., Althausen, D., Wirth, M., Fix, A., Ehret, G., Knippertz, P., Toledano, C., Gasteiger, J., Garhammer, M., and Seefeldner, M.: Depolarization ratio profiling at several wavelengths in pure Saharan dust during SAMUM 2006, Tellus B, 61, 165–179, https://doi.org/10.1111/j.1600-0889.2008.00396.x, http://dx.doi.org/10.1111/j.1600-0889.2008.00396.x, 2009.

Freudenthaler, V., Linné, H., Chaikovski, A., Rabus, D., and Groß, S.: EARLINET lidar quality assurance tools, Atmospheric Measurement Techniques Discussions, 2018, 1–35, https://doi.org/10.5194/amt-2017-395, https://www.atmos-meas-tech-discuss.net/amt-2017-395/, 2018.

Gertisser, R.: Eyjafjallajökull volcano causes widespread disruption to European air traffic, Geology Today, 26, 94–95, https://doi.org/10.1111/j.1365-2451.2010.00757.x, https://onlinelibrary.wiley.com/doi/abs/10.1111/j.1365-2451.2010.00757.x, 2010.

Greed, G., Haywood, J. M., Milton, S., Keil, A., Christopher, S., Gupta, P., and Highwood, E. J.: Aerosol optical depths over North Africa: 2. Modeling and model validation, Journal of Geophysical Research: Atmospheres, 113, https://doi.org/10.1029/2007JD009457, https://agupubs.onlinelibrary.wiley.com/doi/abs/10.1029/2007JD009457, 2008.

Groß, S., Freudenthaler, V., Schepanski, K., Toledano, C., Schäfler, A., Ansmann, A., and Weinzierl, B.: Optical properties of long-range transported Saharan dust over Barbados as measured by dual-wavelength depolarization Raman lidar measurements, Atmospheric Chemistry and Physics, 15, 11 067–11 080, https://doi.org/10.5194/acp-15-11067-2015, https://www.atmos-chem-phys.net/15/11067/2015/, 2015a.

Groß, S., Freudenthaler, V., Wirth, M., and Weinzierl, B.: Towards an aerosol classification scheme for future EarthCARE lidar observations and implications for research needs, Atmospheric Science Letters, 16, 77–82, https://doi.org/10.1002/asl2.524, http://dx.doi.org/10.1002/asl2.524, 2015b.

Guerrero-Rascado, J. L., Barja, B., Lopes, F. J. d. S., Gouveia, D. A., and Barbosa, H. d. M. J.: Latin american lidar network (LALINET) for aerosol research: diagnosis on network instrumentation, JOURNAL OF ATMOSPHERIC AND SOLAR-TERRESTRIAL PHYSICS, https://doi.org/10.1140/epjc/s10052-015-3743-8, 2016.

Guffanti, M., Casadevall, T. J., and Budding, K.: Encounters of aircraft with volcanic ash clouds: A compilation of known incidents 1953-2009, U.S. Geol. Surv., p. 12, 2010.

Hecimovic, A.: Red skies over London - in pictures, The Guardian, 16th October, https://www.theguardian.com/uk-news/gallery/2017/oct/16/red-skies-over-london-in-pictures, 2017.

Holben, B., Eck, T., Slutsker, I., Tanré, D., Buis, J., Setzer, A., Vermote, E., Reagan, J., Kaufman, Y., Nakajima, T., Lavenu, F., Jankowiak, I., and Smirnov, A.: AERONETA Federated Instrument Network and Data Archive for Aerosol Characterization, Remote Sensing of Environment, 66, 1 – 16, https://doi.org/https://doi.org/10.1016/S0034-4257(98)00031-5, http://www.sciencedirect.com/science/article/pii/S0034425798000315, 1998.

Johnson, B., Turnbull, K., Brown, P., Burgess, R., Dorsey, J., Baran, A. J., Webster, H., Haywood, J., Cotton, R., Ulanowski, Z., Hesse, E., Woolley, A., and Rosenberg, P.: In situ observations of volcanic ash clouds from the FAAM aircraft during the eruption of Eyjafjallajökull

in 2010, Journal of Geophysical Research: Atmospheres, 117, https://doi.org/10.1029/2011JD016760, https://agupubs.onlinelibrary.wiley.com/doi/abs/10.1029/2011JD016760, 2012.

Keil, A. and Haywood, J. M.: Solar radiative forcing by biomass burning aerosol particles during SAFARI 2000: A case study based on measured aerosol and cloud properties, Journal of Geophysical Research: Atmospheres, 108, https://doi.org/10.1029/2002JD002315, 2003.

5   Kovalev, V. A.: Lidar measurement of the vertical aerosol extinction profiles with range-dependent backscatter-to-extinction ratios, Appl. Opt., 32, 6053–6065, https://doi.org/10.1364/AO.32.006053, http://ao.osa.org/abstract.cfm?URI=ao-32-30-6053, 1993.

Levin, E. J. T., McMeeking, G. R., Carrico, C. M., Mack, L. E., Kreidenweis, S. M., Wold, C. E., Moosmüller, H., Arnott, W. P., Hao, W. M., Collett, J. L., and Malm, W. C.: Biomass burning smoke aerosol properties measured during Fire Laboratory at Missoula Experiments (FLAME), Journal of Geophysical Research: Atmospheres, 115, n/a–n/a, https://doi.org/10.1029/2009JD013601, http://dx.doi.org/10.

10   1029/2009JD013601, d18210, 2010.

Lewis, J., R. Campbell, J., Welton, E., Stewart, S., and C. Haftings, P.: Overview of MPLNET version 3 cloud detection, Journal of Atmospheric and Oceanic Technology, 33, 2016.

Mallone, S., Stafoggia, M., Faustini, A., Gobbi, G. P., Marconi, A., and Forastiere, F.: Saharan Dust and Associations between Particulate Matter and Daily Mortality in Rome, Italy, 119, 1409–14, 2011.

15   Marenco, F., Johnson, B., Turnbull, K., Newman, S., Haywood, J., Webster, H., and Ricketts, H.: Airborne lidar observations of the 2010 Eyjafjallajökull volcanic ash plume, Journal of Geophysical Research: Atmospheres, 116, https://doi.org/10.1029/2011JD016396, https://agupubs.onlinelibrary.wiley.com/doi/abs/10.1029/2011JD016396, 2011.

Mattis, I., D'Amico, G., Baars, H., Amodeo, A., Madonna, F., and Iarlori, M.: EARLINET Single Calculus Chain – technical – Part 2: Calculation of optical products, Atmospheric Measurement Techniques, 9, 3009–3029, https://doi.org/10.5194/amt-9-3009-2016, https:

20   //www.atmos-meas-tech.net/9/3009/2016/, 2016.

Millington, S. C., Saunders, R. W., Francis, P. N., and Webster, H. N.: Simulated volcanic ash imagery: A method to compare NAME ash concentration forecasts with SEVIRI imagery for the Eyjafjallajökull eruption in 2010, Journal of Geophysical Research: Atmospheres, 117, https://doi.org/10.1029/2011JD016770, 2012.

Nemuc, A., Vasilescu, J., Talianu, C., Belegante, L., and Nicolae, D.: Assessment of aerosol's mass concentrations from mea-

25   sured linear particle depolarization ratio (vertically resolved) and simulations, Atmospheric Measurement Techniques, 6, 3243–3255, https://doi.org/10.5194/amt-6-3243-2013, https://www.atmos-meas-tech.net/6/3243/2013/, 2013.

Osborne, M., Marenco, F., Mariana, A., and Buxmann, J.: Dust Mass Concentrations From the UK Volcanic Ash Lidar Network Compared With In-situ Aircraft Measurements, in: Proceedings of the 28th International Laser Radar Conference, 2017.

Osborne, S. R., Johnson, B. T., Haywood, J. M., Baran, A. J., Harrison, M. A. J., and McConnell, C. L.: Physical and optical proper-

30   ties of mineral dust aerosol during the Dust and Biomass-burning Experiment, Journal of Geophysical Research: Atmospheres, 113, https://doi.org/10.1029/2007JD009551, https://agupubs.onlinelibrary.wiley.com/doi/abs/10.1029/2007JD009551, 2008.

Pappalardo, G., Amodeo, A., Pandolfi, M., Wandinger, U., Ansmann, A., Bösenberg, J., Matthias, V., Amiridis, V., Tomasi, F. D., Frioud, M., Iarlori, M., Komguem, L., Papayannis, A., Rocadenbosch, F., and Wang, X.: Aerosol lidar intercomparison in the framework of the EARLINET project. 3. Ramanlidar algorithm for aerosol extinction, backscatter, and lidar ratio, Appl. Opt., 43, 5370–5385,

35   https://doi.org/10.1364/AO.43.005370, http://ao.osa.org/abstract.cfm?URI=ao-43-28-5370, 2004.

Poudel, S., Fiddler, M. N., Smith, D., Flurchick, K. M., and Bililign, S.: Optical Properties of Biomass Burning Aerosols: Comparison of Experimental Measurements and T-Matrix Calculations, Atmosphere, 8, https://doi.org/10.3390/atmos8110228, http://www.mdpi.com/2073-4433/8/11/228, 2017.

Raut, J.-C. and Chazette, P.: Retrieval of aerosol complex refractive index from a synergy between lidar, sunphotometer and in situ measurements during LISAIR experiment, Atmospheric Chemistry & Physics Discussions, 7, 1017–1065, 2007.

Ryall, D., Derwent, R., Manning, A., Redington, A., Corden, J., Millington, W., Simmonds, P., O'Doherty, S., Carslaw, N., and Fuller, G.: The origin of high particulate concentrations over the United Kingdom, March 2000, Atmospheric Environment, 36, 1363 – 1378, https://doi.org/https://doi.org/10.1016/S1352-2310(01)00522-2, http://www.sciencedirect.com/science/article/pii/S1352231001005222, 2002.

Swap, R. J., Annegarn, H. J., Suttles, J. T., King, M. D., Platnick, S., Privette, J. L., and Scholes, R. J.: Africa burning: A thematic analysis of the Southern African Regional Science Initiative (SAFARI 2000), Journal of Geophysical Research: Atmospheres, 108, https://doi.org/10.1029/2003JD003747, 2000.

Tackamura, T., Nakajima, T., and Group, S. C.: Overview of SKYNET and its Activities, Optica Pura Aplicada, 37, 3303 – 3308, http://www.sedoptica.es/Menu_Volumenes/opavols.php?volumen=37&numero=3, 2004.

Taylor, M., Kazadzis, S., and Gerasopoulos, E.: Multi-modal analysis of aerosol robotic network size distributions for remote sensing applications: dominant aerosol type cases, Atmospheric Measurement Techniques, 7, 839–858, https://doi.org/10.5194/amt-7-839-2014, 2014.

Tesche, M., Ansmann, A., Müller, D., Althausen, D., Engelmann, R., Freudenthaler, V., and Groß, S.: Vertically resolved separation of dust and smoke over Cape Verde using multiwavelength Raman and polarization lidars during Saharan Mineral Dust Experiment 2008, Journal of Geophysical Research: Atmospheres, 114, https://doi.org/10.1029/2009JD011862, http://dx.doi.org/10.1029/2009JD011862, d13202, 2009.

Turnbull, K., Johnson, B., Marenco, F., Haywood, J., Minikin, A., Weinzierl, B., Schlager, H., Schumann, U., Leadbetter, S., and Woolley, A.: A case study of observations of volcanic ash from the Eyjafjallajökull eruption: 1. In situ airborne observations, 117, 2012.

US National Hurricane Center, N.: Former hurricane Ophelia batters Ireland, https://www.nhc.noaa.gov/, 2017.

Woodward, S.: Modeling the atmospheric life cycle and radiative impact of mineral dust in the Hadley Centre climate model, Journal of Geophysical Research: Atmospheres, 106, 18 155–18 166, https://doi.org/10.1029/2000JD900795, https://agupubs.onlinelibrary.wiley.com/doi/abs/10.1029/2000JD900795, 2001.
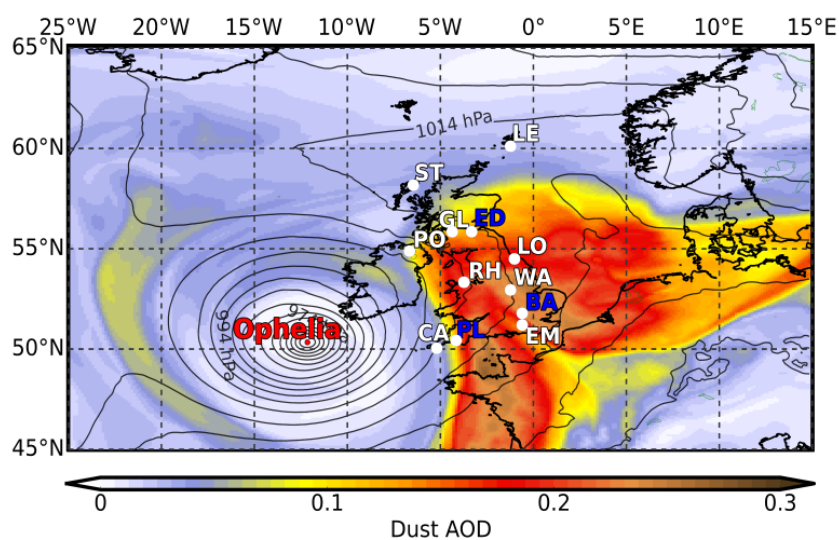
Figure 1. Forecast of dust AOD at 550nm from the Met Office operational Global Model from midnight 13th October 2017, validity time 9am 16th October 2017 (+81 hours). Met Office VA lidar / sun photometer locations are labeled in white. LE = Lerwick, ST = Stornoway, GL = Glasgow, PO = Portglenone, LO = Loftus, RH = Rhyll, WA = Watnall, EM = East Malling and CA = Camborne. Other sun-photometer sites referred to in text are labelled in blue, ED = Edinburgh, BA = Bayfordbury and PL = Plymouth. Lidar sites shown in figure 8 are at Camborne, Rhyl, Watnall (mobile system also located at this site) and Loftus.
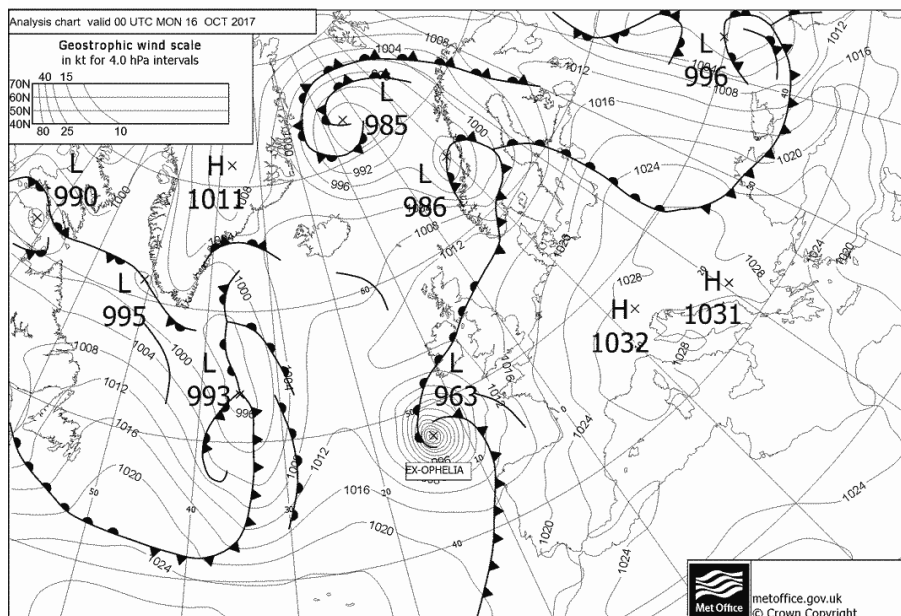
Figure 2. Met Office forecast chart for 00:00 UTC Monday 16th October 2017
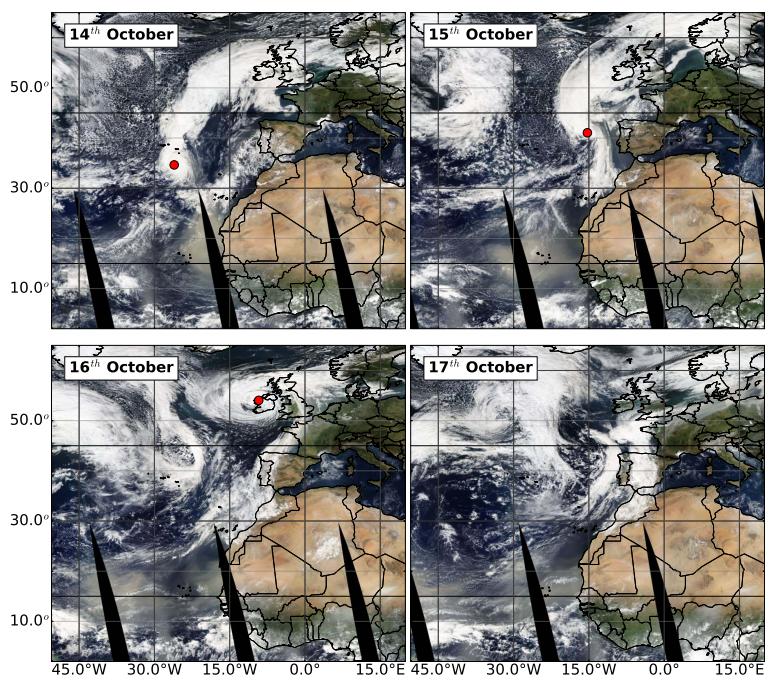
Figure 3. MODIS AQUA composite tiles for the 14th, 15th, 16th and 17th of October 2017. Ex-hurricane Ophelia is highlighted in red.
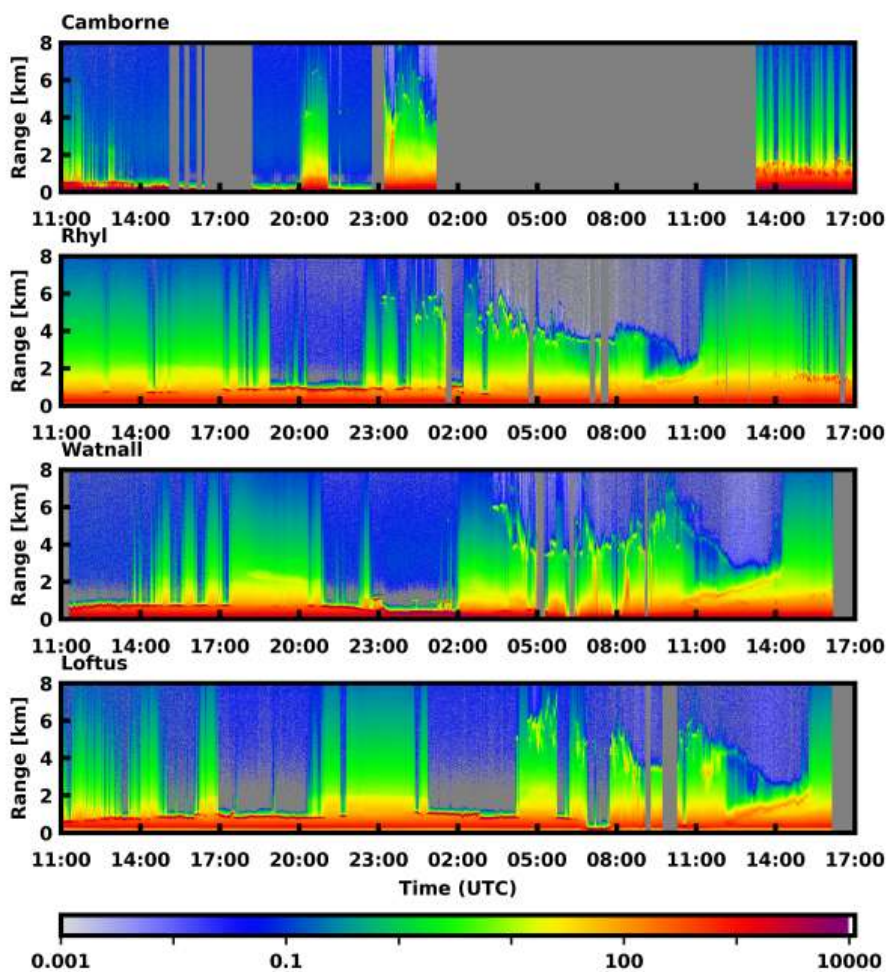
Figure 4. Range corrected signal for the 15th and 16th October 2017, Grey areas indicate no data
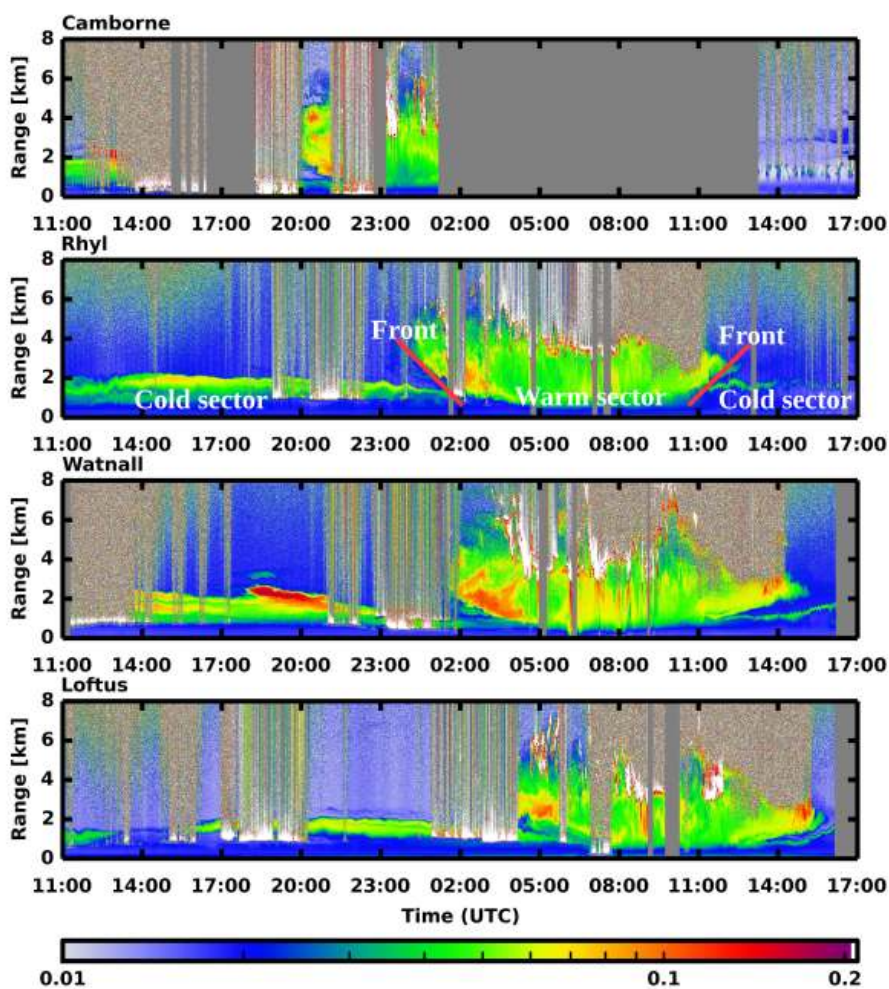
Figure 5. Lidar volume linear depolarisation ratios for the 15th and 16th October 2017, Grey areas indicate no data, and white areas indicate large depolarisation values. An indication of the positions of the cold and warm fronts and sectors are shown on the second panel (Rhyl)
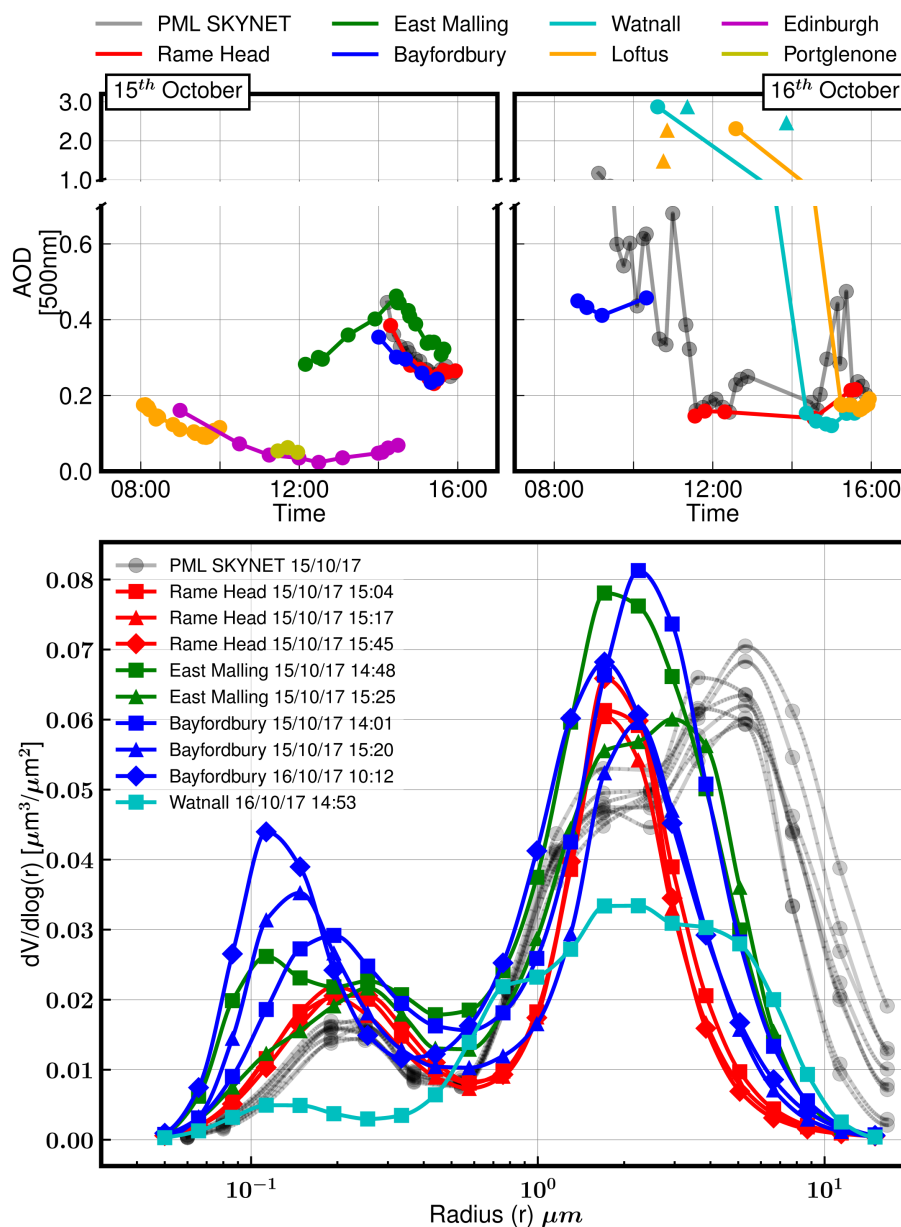
Figure 6. AERONET and SKYNET AODs and volume size distributions
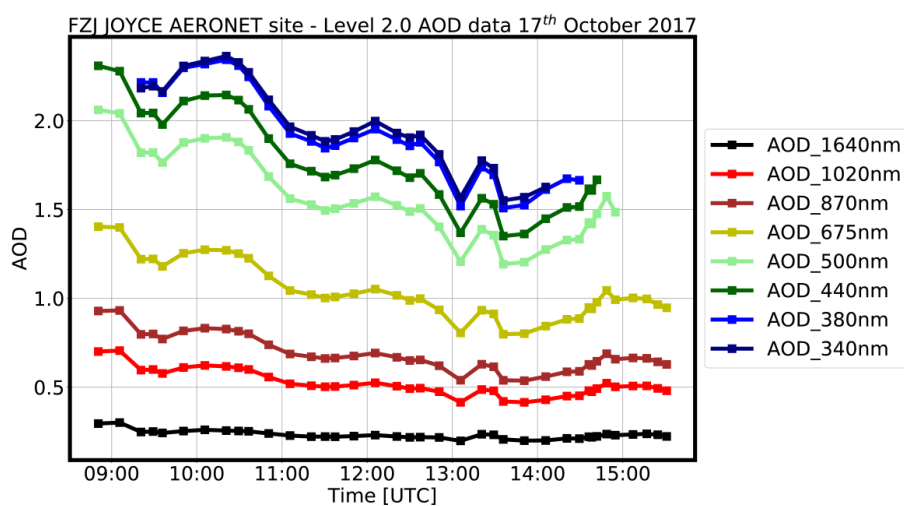
Figure 7. Wavelength variation of AODs measured at the AERONET site in Jülich in Germany on the 17th October 2017. The large wavelength variation seen here indicates that small sub-micron particles have dominated the scattering
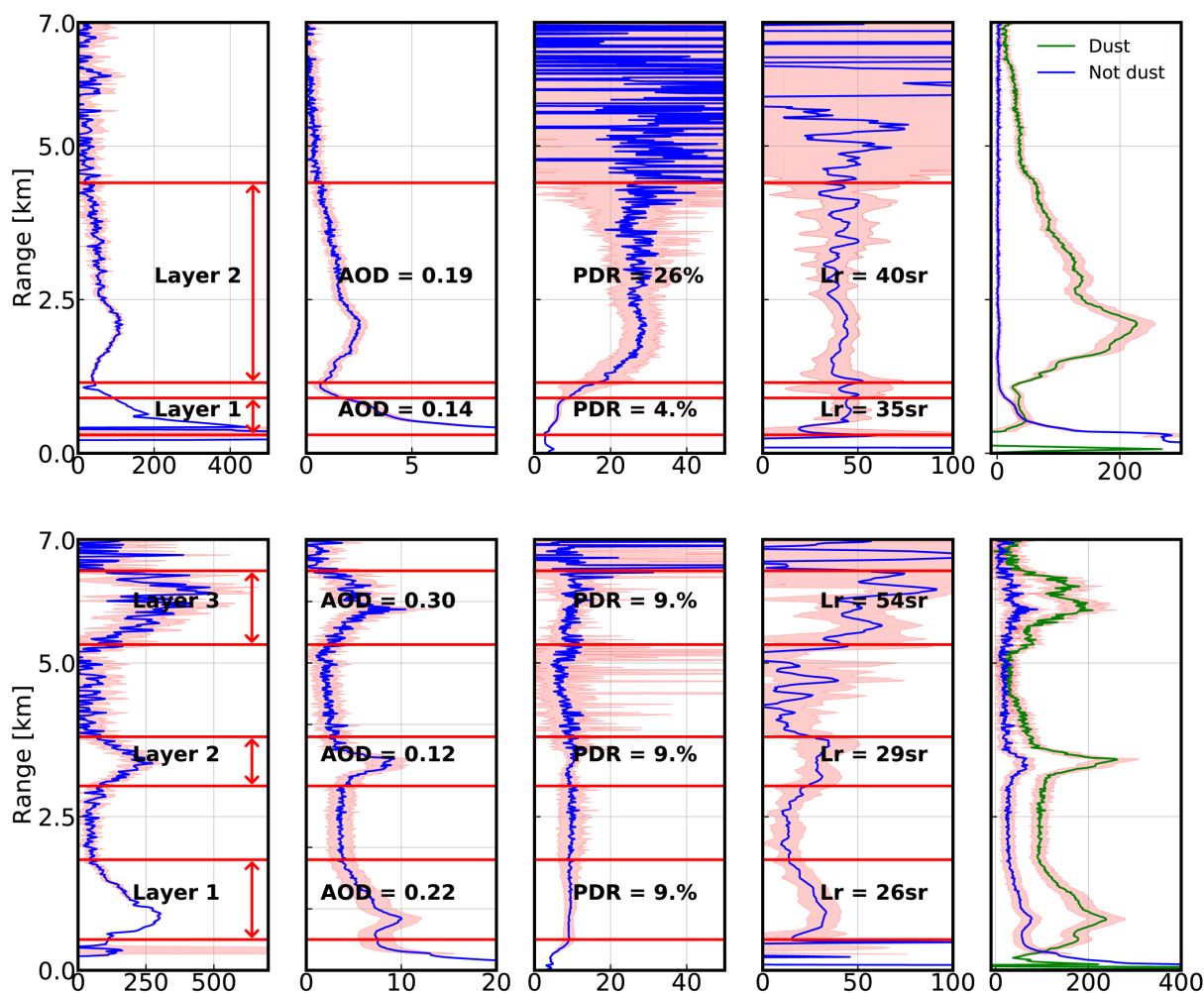
Figure 8. Optical properties and mass concentration estimates calculated from lidar signals. Top row: Watnall 16th October 02:00 to 03:15, bottom row: Watnall 16th October 05:43 to 05:56
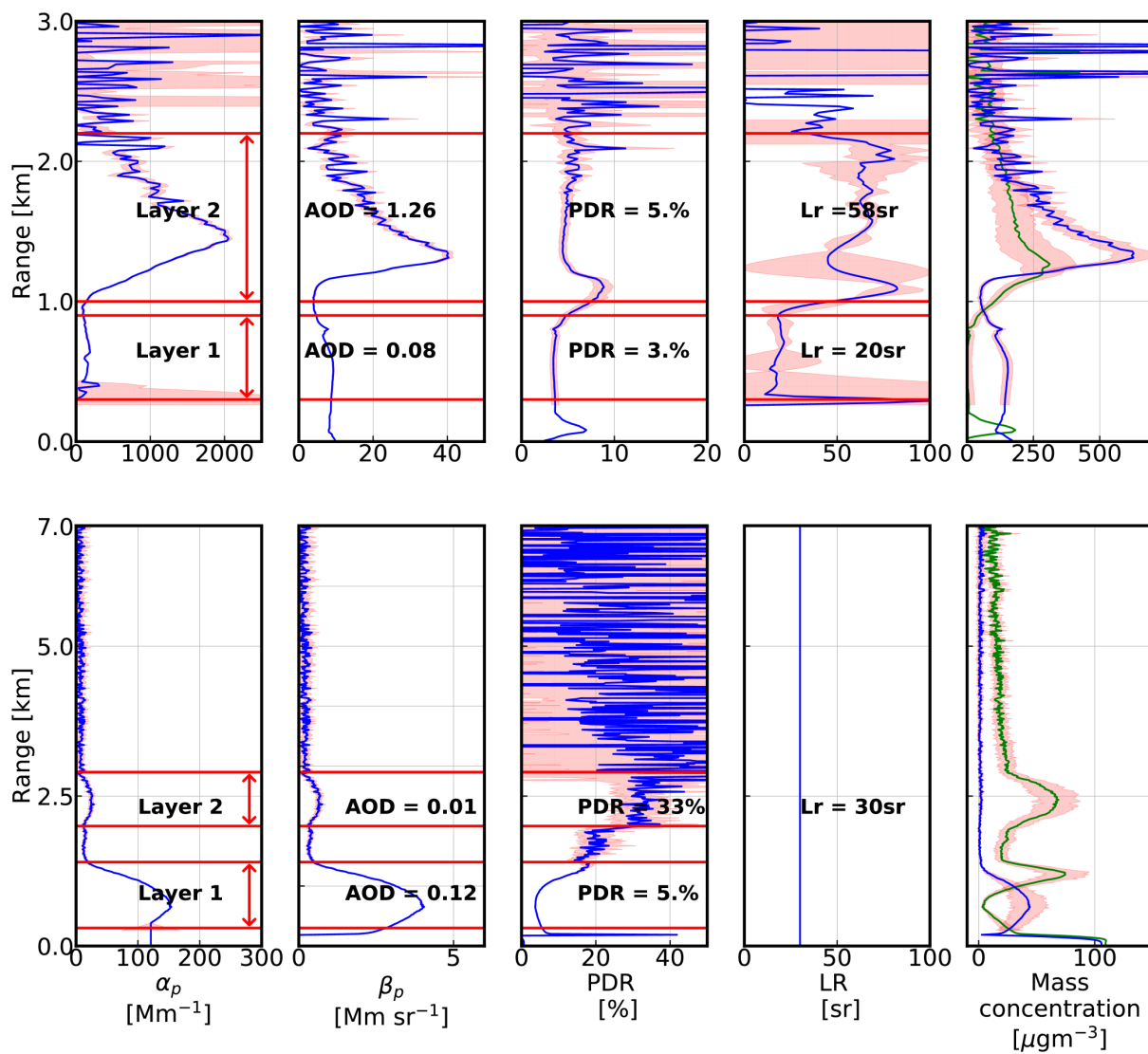
Figure 9. Optical properties and mass concentration estimates calculated from lidar signals. Top row: Watnall 16th October 11:15 to 11:44, bottom row (Fernald / Klett method): Watnall 16th October 14:30 to 15:00
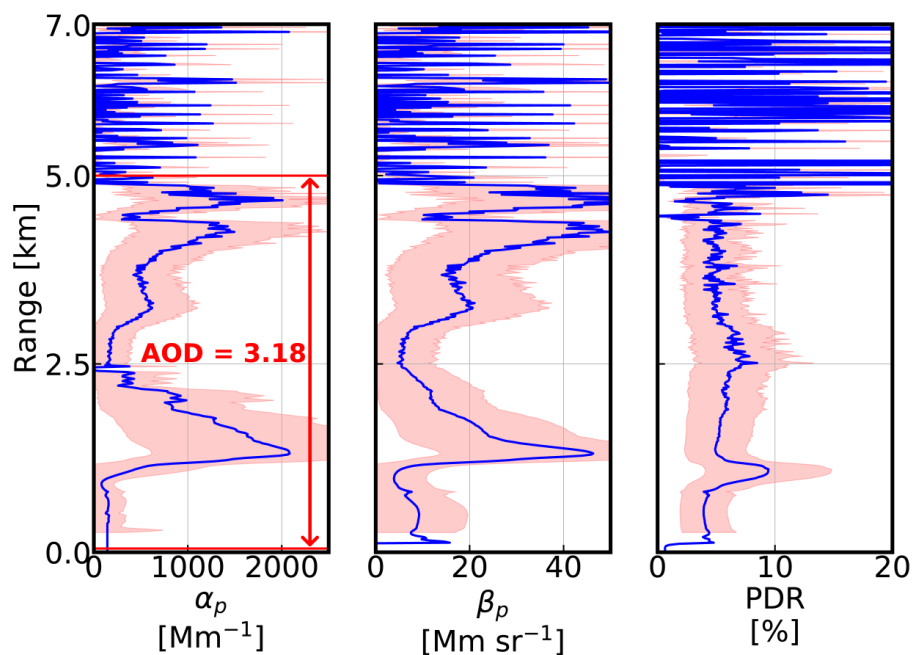
Figure 10. Optical properties calculated from lidar signals using the Fernald / Klett method. Data from Watnall 16th October 11:15 to 11:44. The lidar ratio in the lower 2.5km was set to the height resolved values retrieved using the Raman inversion method (shown in figure 9), above 2.5km the value was set to 40sr. The large errors are a result of the small / noisy signal values at the reference range of 8km, the laser beam having been nearly completely attenuated by the optically thick aerosol layers.
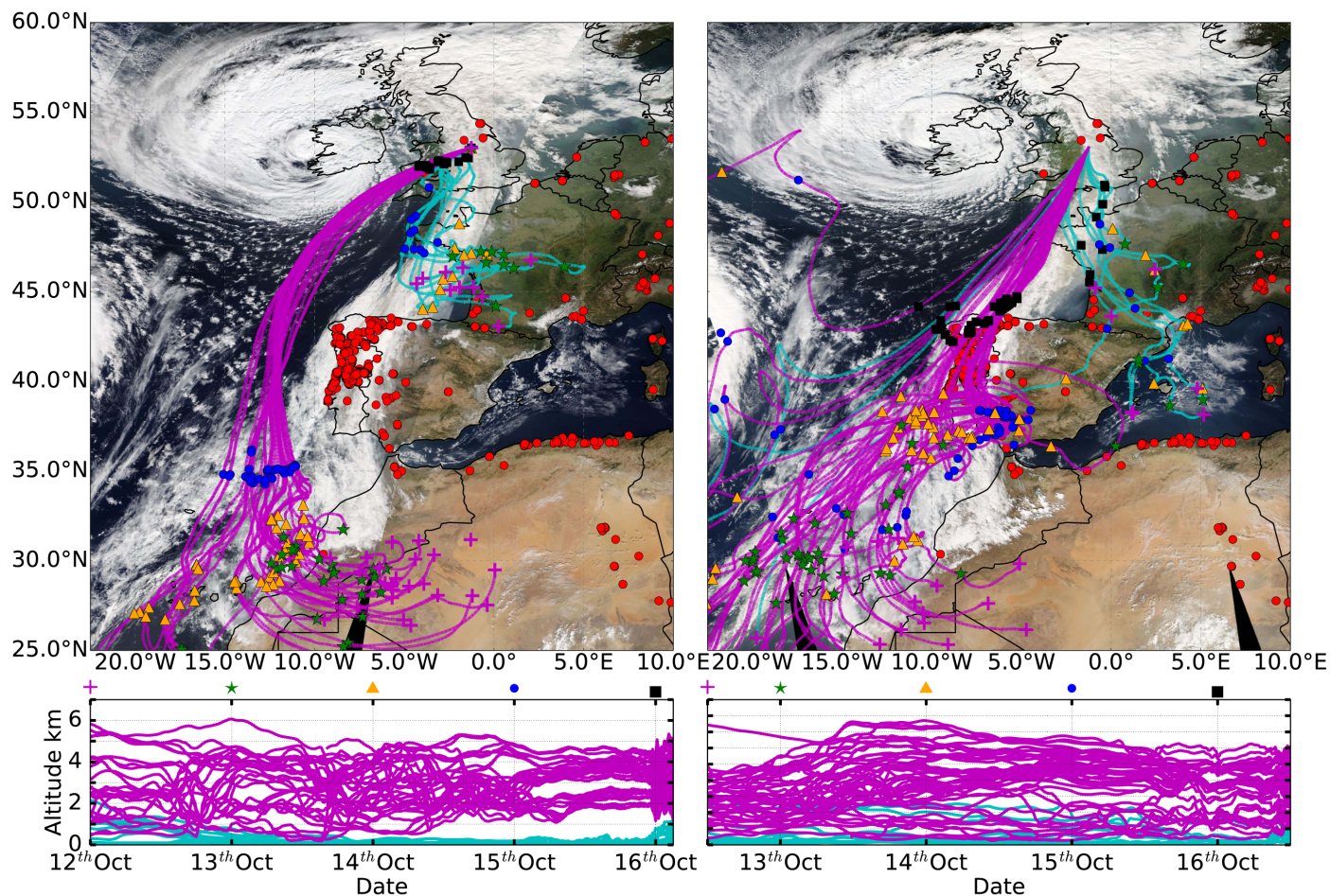
Figure 11. NAME back trajectories overlaid on MODIS AQUA composite image from 16th October 2017. Red dots on MODIS image show active forest fires. Approximate times of overpasses are 1200 UTC for the left hand swath, and 13:45 UTC for the right. In the left (right) hand pannel, back trajectories are for air masses arriving over Watnall at 03:00 UTC (12:00 UTC) on 16th October 2017 at the altitudes shown in the lower panel. Trajectories shown in cyan arrive at Watnall at altitudes under 1km, and trajectories shown in magenta arrive over 1km. The symbols shown on the trajectories themselves and on the top axis of the lower plots indicate the trajectory positions at midnight on each day (with the exception of the purple crosses on the right hand plots, which mark the position at 12:00 UTC on the 12th October).

Table 1. Values of K_{ext} calculated using sun-photometer data

Location	Time & date	K_{ext} [m^{2}g^{-1}]
PML$_{POM}$	14:53 15/10/17	0.41[a]
Rame Head	15:04 15/10/17	0.58
	15:17 15/10/17	0.58
	15:45 15/10/17	0.55
Bayfordbury	14:01 15/10/17	0.53
	15:21 15/10/17	0.56
	10:12 16/10/17	0.65
East Malling	15:04 15/10/17	0.57
	15:45 15/10/17	0.55
Watnall	14:53 16/10/17	0.48

[a]Using T-Matrix calculations.

Table 2. Summary of lidar retrievals. See text for an explanation of sector descriptions

Location	Date	Time	Layer height [km]	PDR [%]	LR [sr]	AOD	Max concentration	Aerosol type
			Initial cold sector					
Rhyl	15/10/17	15:35 to 17:00	0km to 0.75km	8	n/a	0.05	220	Continental pollution/BBA
			0.75km to 2.1km	25	n/a	0.07	170	Dust
Watnall	15/10/17	18:15 to 19:10	0km to 1km	3	37	0.15	150	Continental pollution/BBA
			1km to 2.8km	24	42	0.19	500	Dust
Watnall	15/10/17	19:30 to 20:15	0km to 1km	3	41	0.16	100	Continental pollution/BBA
			1km to 2.2km	24	38	0.19	450	Dust
Loftus	15/10/17	22:30 to 23:59	0km to 1km	5	48	0.07	50	Continental pollution/BBA
			1km to 2km	25	50	0.08	150	Dust
			Warm sector					
Camborne	15/10/17	20:35 to 21:00	0km to 1km	7	42	0.1	320	Continental pollution/BBA
			1km to 5km	24	39	0.21	200	Dust
Watnall	16/10/17	02:00 to 03:15	0km to 1km	3	34	0.15	500	Continental pollution/BBA
			1km to 4.2km	28	40	0.19	220	Dust
Watnall	16/10/17	05:43 to 05:56	0.5km to 1.8km	9	28	0.19	225	Marine/dust
			3km to 3.8km	9	28	0.12	250	Marine/dust
			5.1km to 6.5km	9	51	0.31	200	Dust
Watnall	16/10/17	11:15 to 11:44	0.3km to 0.9km	3	20	0.08	180	Marine
			1km to 2.2km	5	58	1.26	600	BBA/dust
			Final cold sector					
Rhyl	16/10/17	11:15 to 11:40	0km to 1.3km	8	n/a	0.19	75	Continental pollution/BBA
			1.8km to 3km	24	n/a	0.06	150	Dust
Watnall	16/10/17	14:30 to 15:00	0.3km to 1.3km	5	n/a	0.19	75	Continental pollution/BBA
			2km to 3km	33	n/a	0.06	150	Dust
Loftus	15/10/17	15:00 to 15:30	0.3km to 1.1km	4	n/a	0.13	75	Continental pollution/BBA
			1.1km to 2.7km	29	n/a	0.02	100	Dust